Non-nuclear maxima of the electron density on alkaline metals

Víctor Luaña,[a] Paula Mori-Sánchez,[b] Aurora Costales, M. A. Blanco, and A. Martín Pendás
Departamento de Química, Física y Analítica, Universidad de Oviedo, E-33006 Oviedo, Spain

(Received 21 May 2003; accepted 20 June 2003)

The topological properties of the electron density of bcc alkaline metals (Li–Cs) is examined by means of Hartree–Fock and density functional calculations. Our best results indicate that lithium is the only alkaline metal showing non-nuclear maxima (NNM) at the room pressure and temperature experimental geometry. Sodium and potassium, but not rubidium and cesium, would also present NNM under an appropriate compression, even though the NNM in potassium would be residual at best and contain a negligible amount of electrons. Despite these differences, all five alkaline metals share a common tendency towards topological change that makes their behavior clearly distinct from what is typical in ionic, covalent and molecular crystals. When examined in a wide range of interatomic distances, the electron density of every metal follows a well defined topological sequence, with strong similarities across the five metals. © *2003 American Institute of Physics.* [DOI: 10.1063/1.1600433]

I. INTRODUCTION

In any compound, molecule or crystal, nuclear positions are maxima of the electron density. In fact, most of the electron density is accumulated in the close nearby of nuclei, from where it decays exponentially towards the internuclear space. Exceptions to this canon appear, however, under special circumstances. Most notably, additional maxima may appear at non-nuclear positions. The very occurrence of the non-nuclear maxima (NNM) has repeatedly been the subject of controversy.

Early Hartree–Fock (HF) linear combination of atomic orbitals (LCAO) calculations by Besnainou *et al.*[1] found in 1955 the presence of NNM on the Li_2 electron density. Its existence violated the alleged convexity of the electron density in molecular systems, so it was considered a calculation error. That attitude persisted in the early 1980s when Bader *et al.* discovered again the phenomenon in Li_2[2] and acetylene.[3] A collection of works in the 1980s and early 1990s[4–10] made evident that NNM can be very sensitive to the quality of the basis set and, to a less extent, to the correct inclusion of correlation effects. Nevertheless, a final consensus emerged: NNM are stable features on the theoretical electron density of, at less, some small lithium clusters. The extension of this phenomenon to the alkaline crystals appeared as a natural consequence, and HF–LCAO calculations by Mei *et al.*[11] on bcc Li and Na promptly confirmed the suspicion.

The conflict surfaced again on the determination and analysis of the experimental electron density of Li, Be, Na, and Si crystals. Sakata and Sato[12] reported NNM in the electron density of Si, reconstructed with the maximum entropy method (MEM) after the accurate structure factors obtained by Saka and Kato.[13] Similarly, Iversen *et al.*[14] found NNM in the hcp Be density by applying the MEM technique to the structure factors measured by Larsen and Hansen.[15] However, a clever numerical test by de Vries *et al.*[16] proved that the MEM method can be responsible of artifacts in the reconstructed electron density. Namely, de Vries *et al.* showed a NNM lacking theoretical density of Be that was converted, through standard MEM analysis, into a density showing them. The authors remarked[16] that neither a newly proposed weighted MEM method nor their own density functional calculations supported the NNM in Be or in Si. As a reply to these criticisms, Iversen *et al.*[17] performed a detailed Monte Carlo analysis of the errors in the MEM method and concluded that NNM in the Be density are justified well beyond the experimental errors. However, Jayatilaka[18] argued against that conclusion by using a new technique to construct a single Slater determinant wave function for Be from the experimental data by Larsen and Hansen.[15]

In a previous article, we explained partly the reasons behind such controversy[19] through a systematic analysis of the evolution of the electron density of diatomic molecules with the interatomic distance. The shell structure of atoms was shown to be the basic organizing principle underlying the occurrence of NNM. Under the promolecular approximation, homonuclear diatomic molecules exhibit NNM whenever there exists overlap between two regions in which the second radial derivative of the atomic electron density is negative. This atomic feature is carried on to polyatomic molecules and crystals, thus providing a prediction about where NNM should be expected. Self-consistency and correlation effects conserve essentially the promolecular phenomena, increasing slightly the likeness of NNM regions. Therefore, NNM can be viewed as a normal step in the chemical bonding of homonuclear systems but only for an appropriate, usually narrow, range of internuclear distances. For most elements, however, this range occurs far away from the stable geometry under normal thermodynamical conditions. Basis

[a]Author to whom correspondence should be addressed. Electronic mail: victor@carbono.quimica.uniovi.es
[b]Current address: Dept. of Chemistry, Duke University, Box 90354, Durham, NC 27708-0354.

set errors and correlation effects that modify the equilibrium distance of clusters and crystals can produce a lot of confusion by giving rise to wave functions that have or that lack NNM.

Li and Na were proposed in our article among the best candidates to have NNM under room pressure and temperature (RPT).[19] Undetailed CRYSTAL95[20] calculations (later described in Ref. 21) were cited to support the prediction. However, a recent article by Madsen *et al.*,[22] while praising the analysis in Ref. 19, has put in question the predicted existence of NNM in Na. In fact, Madsen *et al.*[22] have obtained what is arguably the best electron density insofar for bcc Li and Na. According to their full potential linear augmented plane wave (FPLAPW) calculations, Li exhibits NNM but Na lacks them under RPT conditions, and only when pressure is significantly increased should the NNM appear on bcc Na.

It is worth mentioning the existence of systems on which NNM are commonly accepted and that have never raised concerns. This is the case of *F* centers[23–25] and electrides.[26] A tantalizing example was created in 1993 by Crommie *et al.*,[27] who built a quantum corral of 48 Fe adatoms on a Cu(111) clean surface. Scanning tunneling microscope images showed the corral's interior local density of states dominated by the eigenstate density expected for an electron trapped in a round two-dimensional box. At variance from simple metals, NNM in the above systems show a significant electron density accumulation compared to their nearby region. On the contrary, the electron density is almost constant throughout the valence region of Li, Na, and other simple metals.[28] This flat valence landscape is at the core of the recurring controversy regarding NNM.

It is our main purpose in this work to contribute towards a definitive answer about the actual existence of NNM in the alkaline metals, from lithium to cesium. To that end we will compare and analyze the outcomes of different computational techniques, both in the crystals and in molecular clusters modeling crystal fragments. We will also analyze the evolution of the crystalline electron density with the interatomic distance, as it has been well established by previous works that the geometry influences markedly the topological properties of the electron density of metals. In anticipation of the forthcoming results, we will show that all five alkaline metals share a common tendency towards topological change as the crystal suffers hydrostatic compression, though every metal has its own particularities in this respect.

The rest of the paper is organized as follows: Section II introduces the different techniques used in this work to determine the electron density and analyze its topological characteristics. The main results obtained for each alkali metal are presented in Sec. III. The similarities and differences among them are examined in Sec. IV, where we also provide evidence showing that the main topological properties are already present in their molecular counterparts. The article concludes with an explicit statement of the topological features that we consider independent from the calculation scheme.

II. METHOD

We have applied four different techniques to obtain the electron density. Firstly, it is obtained under the procrystalline model by adding up together Koga's *et al.*[29–31] nonrelativistic HF radial densities of neutral atoms. We have also used Dovesi's *et al.* CRYSTAL98 code[32] to perform nonrelativistic HF calculations using crystal adapted Gaussian basis sets.[21] Finally, Blaha's *et al.* WIEN97 code[33] has been employed to perform density functional theory (DFT) calculations within the FPLAPW formalism, using either the local spin density approximation (LSDA) with the PW92 functional[34] or the generalized gradient approach (GGA) with the PBE96 functional.[35]

Each of these techniques has strengths and drawbacks that are worth mentioning. The procrystalline model lacks the internuclear electron density accumulation characteristic of true bonding formation, but is able to predict the occurrence of NNM[4,19] and it evolves very smoothly as the interatomic distance changes. The LCAO techniques implemented in the CRYSTAL98 code[32] produce HF or DFT electron densities. However, the use of the rich and flexible bases that are common within the molecular regime usually gives rise to linear dependencies and other technical problems that render the crystal calculation unsuitable. The molecular basis sets must then be truncated and exponents lower than $0.03-0.05\ \mathrm{bohr}^{-2}$, approximately, become forbidden. To compensate this problem, the lowest retained Gaussian exponent is usually massaged or optimized within the crystal. Overall, it is difficult to achieve saturation of the crystal basis set.

The FPLAPW formalism implemented in the WIEN97[33] code establishes a different treatment for nonoverlapping spherical regions close to the nuclei, muffin tins, than for the internuclear regions. Inside each muffin tin, orbitals are described as radial functions times spherical harmonics and a fully relativistic treatment is used, based on the work by Desclaux.[36] The internuclear region is described using plane waves and a scalar relativistic treatment is applied.[37] The wave functions of both pieces are demanded to match on value and slope at the muffin boundaries, but a perfect match would require including spherical harmonics to infinite order within each atomic sphere and a truncated series is used instead. Some care must be taken to ensure that any remaining discontinuity in the density or its slope is not seen by the topological algorithms. As far as we have observed, keeping the muffin tin radii smaller than the smallest distance from a nucleus to any critical point of the electron density is enough for the alkali metals. The actual radii used in our calculations have been: 1.5 (Li), 2.0 (Na), 2.5 (K), 2.5 (Rb), and 2.4 bohr (Cs). We have found, on the other hand, that the electron density topological properties converge quickly with the improvement in the computational parameters, so no further burden is required beyond what is normal in a typical WIEN97 calculation.

With independence of their origin, the electron density of the crystals has been analyzed using our CRITIC[38] quantum theory of atoms in molecules (AIM)[39] topological code. For the purpose of this work it is quite important to determine all the critical points of the electron density. The CRITIC code

TABLE I. Calculated topology for bcc lithium (space group $Im\bar{3}m$) at the RPT experimental geometry ($a=3.51$ Å, Ref. 43). For each CP and computational technique we indicate the kind of CP (left column) and the electron density (right column). In the case of bond CPs we indicate within parenthesis the two CPs connected by the bond path. The values of f, $\mathcal{V}$(Li) and $\mathcal{Q}$(Li) represent the valence flatness (see definition in the text), and the integrated volume and charge within the lithium basin, respectively. All magnitudes are given in atomic units.

Wyckoff's position			Procrystal		HF-LCAO		FPLAPW/LSDA		FPLAPW/GGA	
2*a*	$\mathcal{O}_h$	(0,0,0)	Li	13.817 580	Li	12.886 189	Li	13.562 808	Li	14.018 663
6*b*	$\mathcal{D}_{4h}$	$(0,\frac{1}{2},\frac{1}{2})$	*b*(Li,Li)	0.006 965	*r*	0.007 760	*r*	0.007 356	*r*	0.007 427
8*c*	$\mathcal{T}_h$	$(\frac{1}{4},\frac{1}{4},\frac{1}{4})$	NNM (*n*)	0.007 416	*r*	0.007 225	*r*	0.007 361	*r*	0.007 376
12*d*	$\mathcal{D}_{2d}$	$(\frac{1}{4},0,\frac{1}{2})$	*c*	0.006 964	NNM (*n*)	0.007 792	NNM (*n*)	0.007 384	NNM (*n*)	0.007 463
12*e*	$\mathcal{C}_{4v}$	(*x*,0,0)	*b*(Li,Li)	0.006 965	*b*(Li,r_{6b})	0.007 068	*c*	0.007 236	*c*	0.007 181
16*f*	$\mathcal{C}_{3v}$	(*x*,*x*,*x*)	*b*(Li,*n*)	0.007 411	*c*	0.006 929	*b*(Li,r_{8c})	0.007 261	*b*(Li,r_{8c})	0.007 197
24*g*	$\mathcal{C}_{2v}$	$(x,0,\frac{1}{2})$	—	—	—	—	—	—	—	—
24*h*	$\mathcal{C}_{2v}$	(0,*y*,*y*)	*r*	0.006 965	*b*(*n*,*n*)	0.007 766	NNM (*n*)	0.007 387	*b*(*n*,*n*)	0.007 456
			—	—	*r*	0.007 000	*r*	0.007 252	*c*	0.007 190
48*i*	$\mathcal{C}_2$	$(\frac{1}{4},y,\frac{1}{2}-y)$	—	—	—	—	*b*(n_{24h},n_{24h})	0.007 384	—	—
			—	—	—	—	*r*	0.007 384	—	—
48*j*	$\mathcal{C}_s$	(0,*y*,*z*)	—	—	—	—	*b*(n_{12d},n_{12d})	0.007 384	*r*	0.007 190
48*k*	$\mathcal{C}_s$	(*x*,*x*,*z*)	—	—	—	—	—	—	—	—
96*l*	$\mathcal{C}_1$	(*x*,*y*,*z*)	—	—	—	—	—	—	—	—
		f (%)		93.97		89.23		97.96		96.31
		$\mathcal{V}$(Li) (%)		80.8		23.5		30.2		26.3
		$\mathcal{Q}$(Li)		0.202		0.831		0.748		0.792

implements several analytical techniques to this end.[40–42] A necessary condition for the complete set of critical points is the fulfillment of Morse's relationships

$$n-b+r-c=0, \tag{1}$$

and

$$n\geqslant 1,\ b\geqslant 3,\ r\geqslant 3,\ c\geqslant 1, \tag{2}$$

where n, b, r, and c are, respectively, the total number of local maxima (nuclei and NNM), bond, ring, and cage (local minima) critical points of the electron density in the crystal unit cell.

III. RESULTS

A. Lithium

To start with, let us examine the electron density topology of bcc lithium at the experimental RPT geometry quoted in Ref. 43. Table I presents the electron density values at the critical points for the procrystalline, HF–LCAO, FPLAPW LSDA, and GGA calculations. The very first thing to notice is that each computational technique predicts a different topology. However, all of them contain NNM. The procrystalline model shows NNM on the midpoint of the Li–Li nearest neighbors lines (Wyckoff's 8*c* position). HF–LCAO and FPLAPW/GGA agree on predicting the NNM to reside on the 12*d* position, but their topologies differ in, for instance, the number and position of bond CPs. Finally, the FPLAPW/LSDA calculations show two types of NNM, one at 12*d* and the second one at the interstitial 24*h* position.

This striking variability is closely related to the fact that the electron density is nearly flat, almost a constant, for most of the internuclear region. An appropriate measurement of the valence flatness is provided by the ratio[28]

$$f=\frac{\rho_c^{\min}}{\rho_b^{\max}}, \tag{3}$$

where $\rho_c^{\min}$ is the absolute minimum of the electron density (necessarily a cage CP), and $\rho_b^{\max}$ is the maximum electron density found among the bond CP's. Typical covalent, ionic and molecular solids have f values quite close to zero. Alkali metals, on the contrary, approach $f=100\%$ and truly resemble the ideal Drude model of a free electron gas. For instance, our FPLAPW calculations on bcc lithium predict f to be 98% (LSDA) or 96% (GGA). In addition, we have found that the value of f is sensitive to the variational flexibility of the LCAO or FPLAPW calculations. When lacking the appropriate flexibility, calculations tend to accumulate the valence density more around the bond CPs, where it contributes most to the energy, at the expense of the ring and cage CP neighborhoods. The use of a well saturated basis set (LCAO calculations), or of a saturated set of plane waves plus a large enough collection of spherical harmonics within the muffin spheres (FPLAPW calculations) prevents this problem, and makes f converge quickly to its physically significant value.

For the rest of this section we will restrict the discussion to the FPLAPW/GGA calculations, that constitute our best effort in terms of flexibility and overall quality. Figure 1 shows the topological graph and the shape of lithium and NNM attraction basins calculated at the experimental geometry. It can be readily observed that NNM are situated at interstitial positions, they form a connected three dimensional network that occupies about 74% of the bulk volume and receives about 0.79 electrons from each Li atom. On the other hand, the Li basins appear as featureless spheres filling only some 26% of the crystal volume. The topological graph and the basin shapes closely resemble the typical aspect of

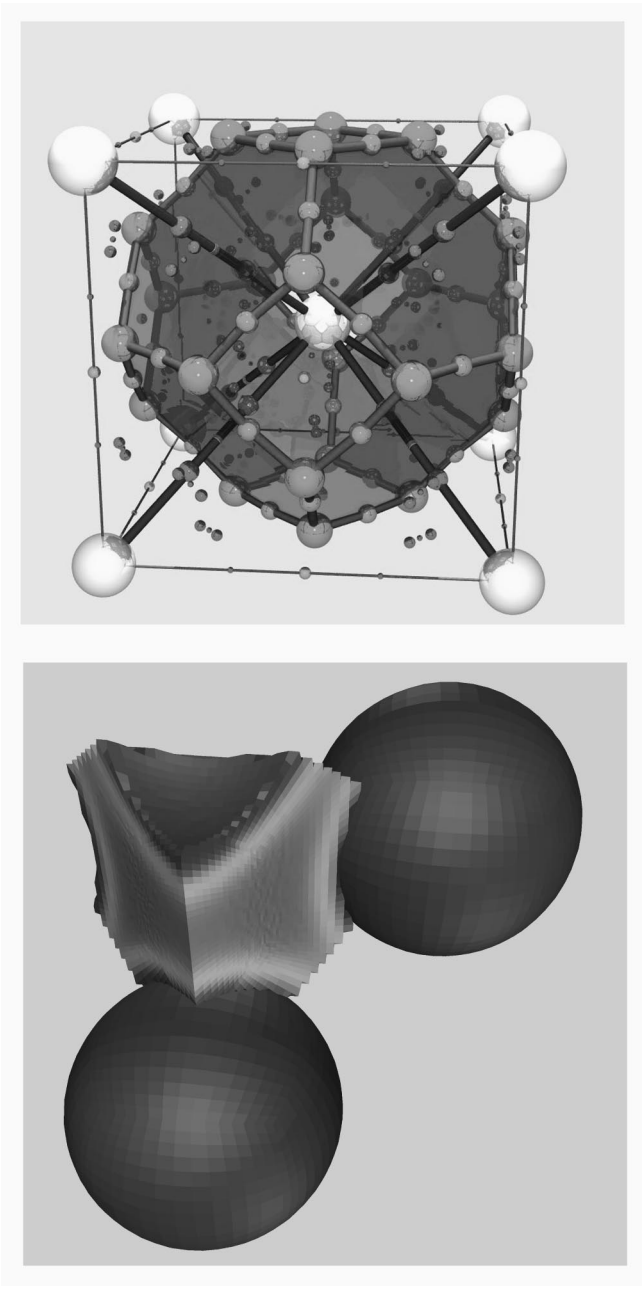

FIG. 1. (Left) Topological graph of the FPLAPW/GGA electron density of lithium at the RPT experimental geometry. Balls of decreasing size represent Li, NNM, bond, ring and cage CPs, respectively. Bond paths are represented as thick pipes connecting the bonded CPs. The NNM form a three dimensional bonded network. Each lithium core lies in the middle of a cuboctahedron of NNM, being bonded to the ring CP's that occur at the hexagonal faces. The plot has been designed using TESSEL (Ref. 53) and rendered with POVRay (Ref. 54). (Right) Detail of the attraction basins of two lithium cores (the spheres) and a NNM according to the FPLAPW/GGA calculation. The concave interatomic surfaces in the NNM basin correspond to the contact with the lithium cores, and the planar ones to the NNM–NNM bonding surfaces. The rendering has been done using GEOMVIEW (Ref. 55).

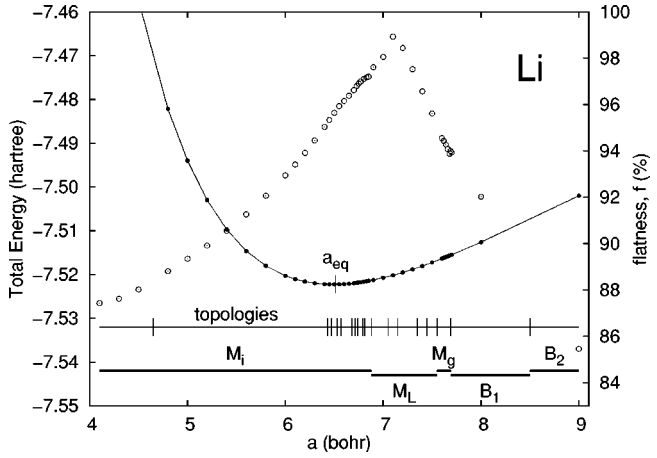

FIG. 2. Summary of the FPLAPW/GGA calculations on bcc lithium. The properties represented are: total energy (solid line and black dots), electron density flatness (empty circles), range of existence of each detailed topology, and of each topological regime (see text for the definition of B_1, B_2, M_g, etc).

ionic crystals, with the Li core playing the role of the hard cation and the NNM acting as soft, polarizable anions.[40] At difference from ionic crystals, however, the valence electron density of Li is flat, as discussed before.

An interesting feature of the topological graph deserves further attention. As Fig. 1 shows, there is no NNM–Li bond path. Rather, the Li cores are bonded to ring CPs placed at the middle of hexagonal arrangements of NNM. This connectivity, that would be typical of a metallocene, can only be maintained as far as the symmetry of the bcc lattice is forced in a static calculation. The introduction of vibrational displacements will cause the reordering of NNM and bond CPs. Moreover, the extreme flatness of the electron density valence gives rise to a significant topological variability that we will examine by modifying the lattice parameter while keeping the bcc structure.

Figure 2 presents our FPLAPW/GGA results for an ample range of lattice parameters (a), 4.1–12 bohr. The equilibrium values for a and the bulk modulus, 6.489 bohr and 13.1 GPa, respectively, do compare well with the experiments, 6.5704 bohr at 20 K[44] and 12.55 GPa (Ref. 45, extrapolated to 0 K). Up to 19 different topologies have been found for the electron density, but this list might not be exhaustive, as our 43 geometries grid is perhaps not thin enough. The important thing, however, is that those 19 topologies are far from chaotic. Rather, they can be grouped into five different significant families with the following properties: B_2: first and second neighbors Li–Li bond CPs occur at $8c$ and $6b$ Wyckoff's positions, respectively; B_1: only nearest neighbors Li–Li bond CP remains at $8c$ position; M_g: twin NNM appear on the nearest neighbors Li–Li line ($16f$ position); M_L: the twin NNM coalesce with a bond CP and a single NNM remains at Wyckoff's $8c$ position, still within the nearest neighbors Li–Li line; and M_i: finally, the NNM move towards interstitial places, first wandering through positions $48i$ and $48j$, at least, but finally occupying the so called tetrahedral hole position ($12d$), where they remain stable up to the lowest lattice parameters explored here.

These five topological families, which can be interpreted as stages in the formation of the metallic bonding, appear successively when the lattice parameter decreases. It is suggestive that most of the topological changes occur for lattice parameters in the range 6.4–7.5 bohr, where the valence

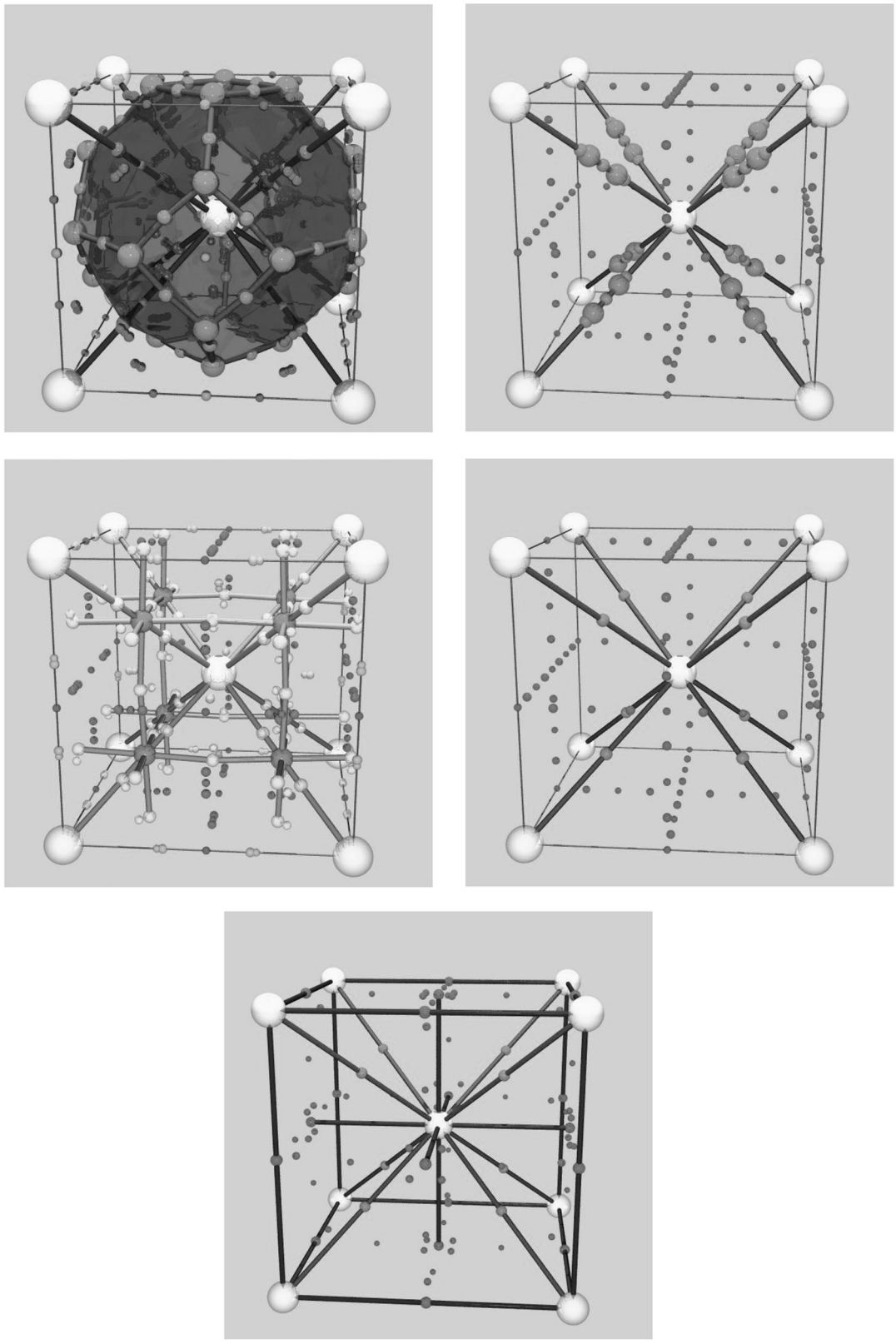

FIG. 3. From left to right, topological graphs representative of the M_i, M_L, M_g, B_1, and B_2 topological families. The same conventions are followed as in Fig. 1.

electron density flatness is 95%–99%, extremely close to that of a free electron gas. A representative topological graph for each family is depicted in Fig. 3. It can be observed that the nearest neighbors Li–Li line remains a bond path for all topologies. The topology at the equilibrium distance belongs to the M_i family.

Similar results can be found for all the computational techniques examined in this work. Compared to the GGA

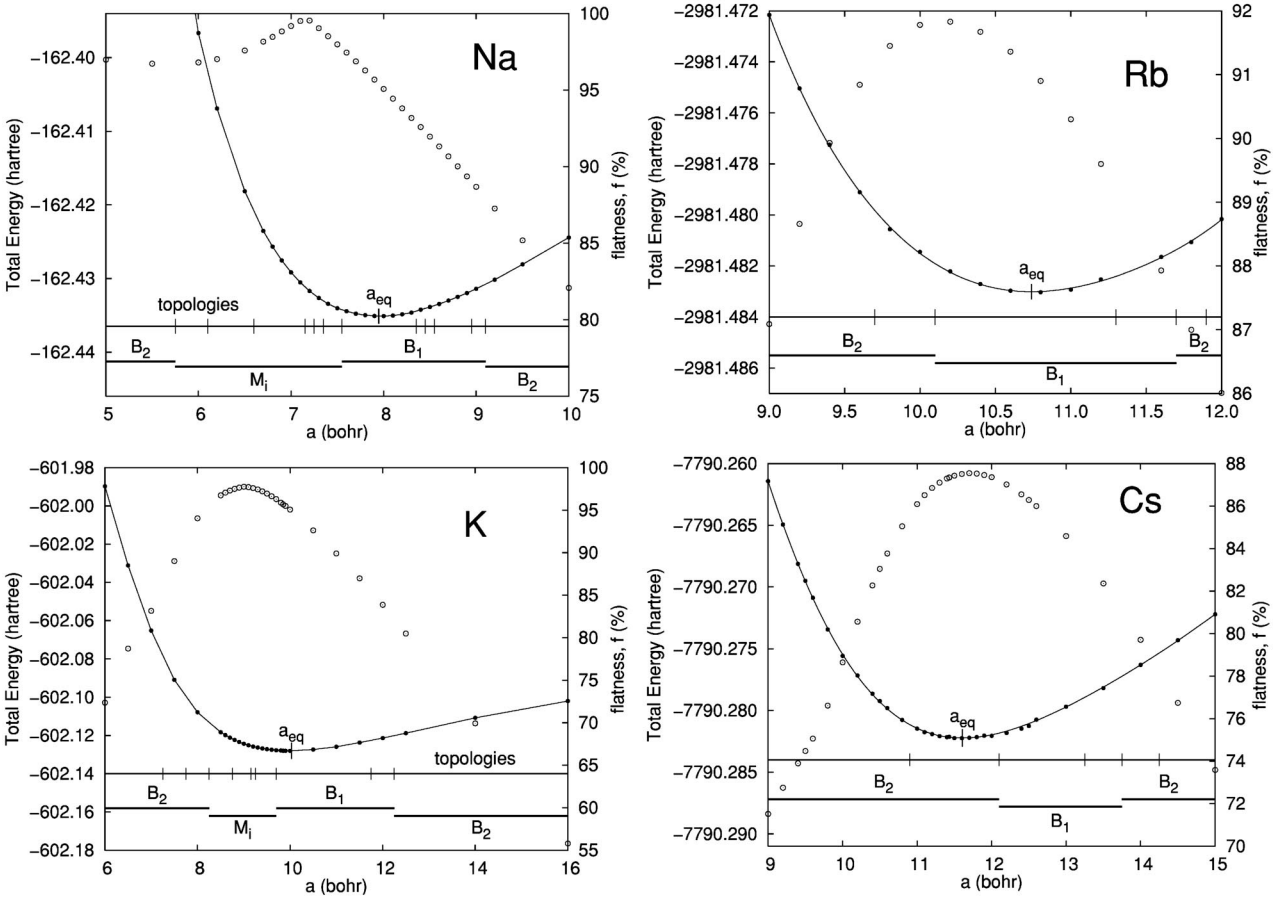

FIG. 4. Summary of the FPLAPW/GGA calculations on bcc sodium, potassium, rubidium, and cesium.

calculations, the FPLAPW/LSDA topologies and equilibrium geometry appear shifted toward shorter distances. Even more shifted are the topologies obtained from the procrystalline model, according to which NNM appear for a crystal compression quite close to the experimental distance. Finally, the HF–LCAO topologies are dependent on the basis set used in the calculation, particularly on the actual value of the smallest Gaussian exponent, but unequivocal NNM were predicted for whatever realistic basis set we have used.

The change from one topology to another deserves further attention. First, it is clear from Fig. 2 that there is no gap between the topologies that show NNM at different positions. On the other hand, there are reasons to believe that NNM should disappear at very short lattice parameters.[19] The procrystalline model predicts that this should happen at $a \approx 4.4$ bohr, but we have not found it yet at 4.0 bohr in our FPLAPW calculations. Finally, all changes in the topology occur either as two or more CP's approach up to coalesce into a single position, or just the opposite. These processes correspond to elementary catastrophes in the sense defined by René Thom.[46] A detailed analysis of the catastrophes occurring to the procrystalline electron density of lithium can be found in Ref. 21. What is more relevant here is that the electron density evolves smoothly as the lattice parameter changes, and the same happens to the FPLAPW results as far as our grid of geometries has allowed us to check.

B. Sodium

Let us examine now in some detail the case of bcc sodium, as it has generated some controversy. At difference from lithium, the procrystalline electron density of sodium lacks NNM for all lattice parameters in the range 4–18 bohr. This is not what happens with the densities coming from the true electronic structure calculations. The three techniques employed in this work predict a range of occurrence of NNM that starts quite close to the corresponding equilibrium geometry. In the case of the HF–LCAO calculations, the onset for the appearance of NNM is quite sensitive to the basis set, particularly to the actual value of the lowest Gaussian exponents. A careful optimization of these exponents tends to displace the appearance of the NNM towards geometries slightly more compressed than the equilibrium or the experimental distance under room pressure and temperature. This is in agreement with the prediction of the FPLAPW calculations using either the LSDA or GGA approximation. This is also in agreement with the results reported by Madsen *et al.*[22]

The results of our best FPLAPW/GGA calculation are gathered in Fig. 4. NNM appear for a compression $V/V_{eq} \approx 0.844$. This corresponds to applying an hydrostatic pressure of 1.4 GPa, according to the equation of state obtained from our theoretical $E(V)$ values by applying the quasihar-

monic Debye technique described in Ref. 47. This pressure is easily attained in the laboratory. According to Fig. 4, NNM exist when the lattice parameter lies in the range 7.51–5.75 bohr, which corresponds to 1.4–40 GPa. The electron density of sodium follows a sequence similar to that of lithium as the lattice parameter decreases: $B_2 \rightarrow B_1 \rightarrow M_i \rightarrow B_2$. Two significant differences stand out, however. First, NNM appears directly on the interstitial positions of the sodium crystal, and the intermediate M_g and M_L stages are absent here. Second, the range for the existence of NNM is shorter and we have been able to see its disappearance.

C. Potassium, rubidium, and cesium

Compared to lithium, we have seen that the range of existence of NNM in sodium is much decreased. This trend continues in the case of potassium, rubidium, and cesium. Acording to the FPLAPW/GGA results represented in Fig. 4, potassium exhibits NNM for a very reduced interval of about 1.4 bohr that starts slightly below the equilibrium geometry, and rubidium and cesium finally lack NNM. Despite these differences, it is interesting to observe how the five alkali metals behave in a similar way regarding the evolution of the electron density flatness. In going from the large distance regime to the short lattice parameters, the value of f increases, reaches a maximum and decreases quickly. At the peak, which is reached slightly before the equilibrium distance in lithium and slightly after it in the remaining cases, the f value is 98%–100% for Li–K, 92% for Rb, and 88% for Cs. This behavior suggests that a very large f value is needed before NNM could appear in these metals.

A second point of coincidence between the different metals is worthy of attention. All alkali metals show a large tendency towards topological change that makes them apart from covalent, ionic and molecular compounds. The NNM are absent from Rb and Cs due to the insufficient electron density flatness, and the occurrence of NNM first along the Li–Li nearest neighbors line before moving to interstitial positions seems to be a particularity of lithium. Aside from those small deviations, the implicit general trend is that compression induces a well defined sequence of topological changes: $B_2 \rightarrow B_1 (\rightarrow M_i) \rightarrow B_2$.

Let us end this section by examining two significant properties of NNM, namely how much charge they accumulate and what a portion of the crystal volume is occupied by them. Figure 5 depicts both properties for Li–K. The difference between the three crystals is astounding. Whereas the lithium atom transfers about $0.79\,e$ to the NNM, that fill some 74% of the crystal volume, the transference is way less important in sodium ($0.30\,e$ and 25% utmost), and almost negligible in potassium ($0.05\,e$ and 4% at the peak). This tells clearly that the occurrence and extent of NNM depend heavily on the atomic number, being the lighter elements are far more prone to show them.

IV. DISCUSSION

After examining the evidence regarding the occurrence of NNM on some alkali metals we want to move our attention towards the causes of the phenomenon. Bersuker *et al.*[10] have tried to explain NNM as a consequence of the electron–electron mediated coupling to low lying excited states, which brings the authors to predict that weak long bonds between atoms with low electronic excitation energies are best suited to display NNM. However, even the procrystalline electron densities are able to show NNM, a fact first shown by Spackman and Maslen,[4,48] and this should lead us to prefer a simpler explanation, well rooted into the atomic properties.

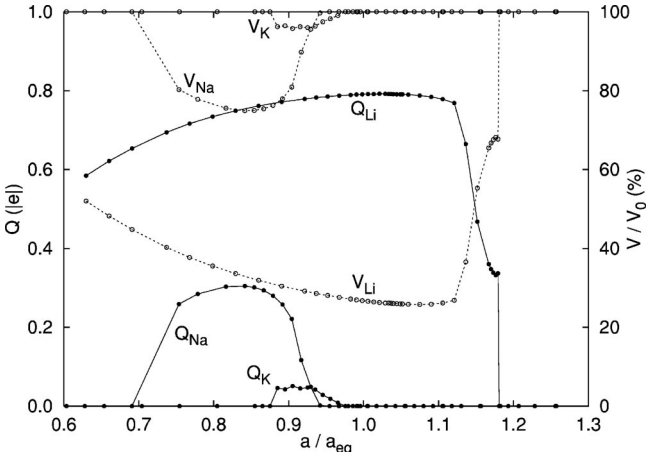

FIG. 5. Charge and volume occupied by NNM in bcc lithium, sodium, and potassium.

In seeking for such an explanation, we will test a collection of approximate models of the crystalline density. The models are based on two simple ideas well supported by the empirical evidence. First, the behavior of the electron density at a given point is dominated by the contribution of a few atoms, the closest ones to the point. Therefore, we will examine the M_2 diatomic molecule and a M_4 elongated tetrahedron cluster as representations of the $M-M$ nearest neighbors line and Wyckoff's $12d$ position, respectively. Both molecules constitute the simplest and most useful portions of the crystal to look at, according to the results described in the previous section. Second, the electron density of a free atom (or ion) remains largely unmodified when entering into a molecular or crystalline compound. Accordingly, the electron density of the M_2 and M_4 groups will be analyzed first by using the promolecular model and then by performing actual self-consistent calculations.

Within the promolecular (or procrystalline) model, the electron density at a given point, $\mathbf{r}$, is obtained as

$$\rho(\mathbf{r}) = \sum_i \rho_i(|\mathbf{r}-\mathbf{r}_i|), \tag{4}$$

where ρ_i is the radial density of the atom situated at $\mathbf{R}_i$. Two metal atoms dominate the properties along the $M—M$ nearest neighbors line (Wyckoff's $16f$ position) and, particularly, at its midpoint (the $8c$ position) a critical point enforced by symmetry. The curvatures of the electron density at this midpoint are given, in the M_2 homodiatomic promolecule, by

$$\rho''_{\parallel} = 2\rho''_M(r), \tag{5}$$

$$\rho''_{\perp} = 2\rho'_M(r)/r, \tag{6}$$

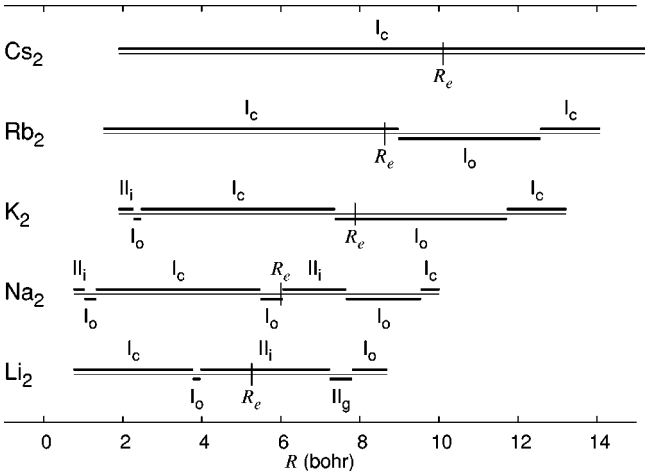

FIG. 6. Topological properties of the electron density of the alkaline diatomic molecules. R_e is the equilibrium distance. The topological regions are named according to the notation described in the text. All results correspond to CISD calculations. TZV+$(3d,1f)$ basis sets have been used in Li_2 (Refs. 56 and 57), Na_2 (Refs. 57 and 58), and K_2 (Refs. 57 and 59). 3-21G$(1d)$ basis sets have been used in Rb_2 (Refs. 60 and 61) and Cs_2 (Refs. 61 and 62). The GAUSSIAN 98 code (Ref. 63) has been used to obtain the wave function and the AIMPAC suite (Ref. 64) to determine its topological properties.

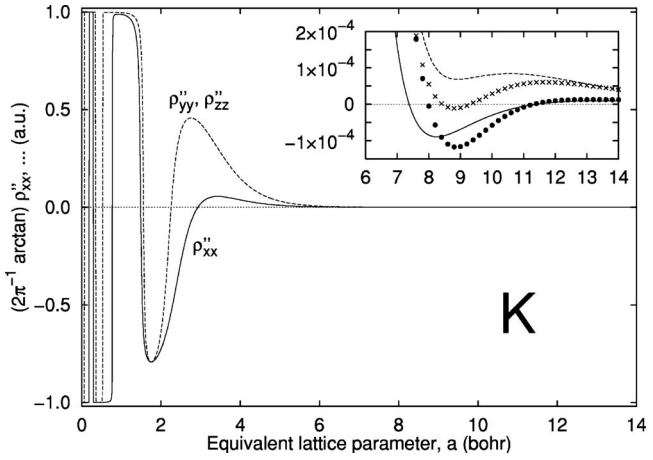

FIG. 7. Curvatures of the electron density of potassium at the center of a K_4 elongated $\mathcal{D}_{2d}$ tetrahedron cluster representative of Wyckoff's $12d$ position in the bcc crystal. Solid and dashed lines correspond to promolecular values, whereas the CISD/TZV+$(3d,1f)$ results are represented with crosses and filled circles (in the inset). The curvature values are represented in the form $\arctan(\rho''/1\text{ a.u.})/(\pi/2)$ in order to map the open range $(-\infty,\infty)$ to a simpler $[-1,1]$ closed one. This mapping displays with negligible deformation the positive and negative low curvature regions. NNM are predicted in this position if lattice parameters smaller than 1 bohr could be achieved. The GAMESS code (Ref. 65) has been used to obtain the wave function and the AIMPAC suite (Ref. 64) to determine its topological properties.

where $\parallel$ and $\perp$ represent the parallel and perpendicular directions to the $M-M$ line, respectively; $\rho'_M(r)$ and $\rho''_M(r)$ are the first and second radial derivative of the atomic density of M; and $r=d(M,M)/2$ is the distance from M to the midpoint. For all atoms $\rho'_M(r)<0$ and, accordingly, Wyckoff's $8c$ position should be either a bond critical point [if $\rho''_M(r)>0$, i.e., the atomic density is convex] or either a NNM [if $\rho''_M(r)<0$]. Most of the alkaline metals correspond to the first case. The exception is lithium which, for a large range of distances, becomes concave.[49,50] The potassium atom shows also regions of concavity, but only for distances of 0.9–1.1 bohr, much smaller that those found in the metal.

Self-consistency and correlation effects produce small modifications on the promolecular image. Figure 6 portrays the different topologies found on the configuration interaction including single double excitations (CISD) calculations of the alkaline homodiatomic molecules at different internuclear separations. We can distinguish four topological regimes: I_c: The midpoint is a bond CP with a positive value for the electron density Laplacian, $\nabla^2\rho(\mathbf{r}_b)>0$, thus characterizing the $M-M$ bonding as a closed shell interaction;[39] I_o: The midpoint is again a bond CP, but the Laplacian is negative and has the properties of a shared shell interaction,[39] albeit a weak one; II_g: Twin NNM appear along the $M-M$ line. The sequence of CPs along the $M-M$ line is: M–bond–NNM–bond–NNM–bond–M. Bonding between the NNM is characterized by a negative Laplacian, whereas bonding to the M core presents usually a positive Laplacian; and II_i: The midpoint is a NNM. Accordingly, the following sequence of CPs can be found in the $M-M$ line: M–bond–NNM–bond–M.

The regime of twin NNM occurs exclusively for a short range of distances in the case of the Li_2 molecule, as it was first described by Cioslowski.[7] Li_2 and Na_2 show NNM at or quite close to the equilibrium distance. K_2 presents NNM but only for very short internuclear separations, around one fourth of the equilibrium distance. Finally, neither Rb_2 nor Cs_2 have NNM for internuclear distances larger than 2 bohr. It is quite interesting that, beyond the actual differences, we can identify a common trend in the evolution of the density for all five molecules. As we go from larger to smaller internuclear distances, the atomic valences interact to produce the following sequence of topologies: $I_c\rightarrow I_o\rightarrow(II_g,II_i\rightarrow I_o)\rightarrow\ldots$. Here, the occurrence of NNM is a particularity of some homodiatomic molecules but, in all cases, the sequence is repeated successively as the internuclear distances decrease and the inner electronic shells pass to dominate the atomic interaction. In fact, this sequence is not exclusive of the alkaline metal diatomic molecules, but it can be shown to be a general scheme closely followed by most homodiatomic systems.[51]

Let us turn now to examine Wyckoff's $12d$ position, which is surrounded by four M atoms forming the corners of an elongated $\mathcal{D}_{2d}$ tetrahedron. The promolecular model predicts the following curvatures for the electron density at the tetrahedron's baricenter:

$$\rho''_{xx}=\tfrac{4}{5}(\rho''_M(r)+4\rho'_M(r)/r), \tag{7}$$

$$\rho''_{yy}=\rho''_{zz}=\tfrac{4}{5}(2\rho''_M(r)+3\rho'_M(r)/r). \tag{8}$$

The $12d$ position can thus be any type of critical point depending on the actual sign of both types of curvatures. The promolecular model predicts that all five alkaline metals have regions in which the three curvatures are negative and thus the $12d$ position becomes NNM. Such regions, however, are usually associated to the inner or core shells (see the case of potassium in Fig. 7) and are not relevant in es-

tablishing the physical properties under reasonable compression. The exception is lithium, that shows a valence region ($a=4-6$ bohr) with all curvatures negative. In the case of sodium, ρ''_{xx} is negative for lattice parameters in the range 5–9 bohr, and $\rho''_{yy}=\rho''_{zz}$ become negligible around 6 bohr.

The promolecular curvatures at the 12*d* position can be refined by doing actual quantum mechanical calculations on the M_4 cluster model. Either HF or CISD calculations decrease all curvatures in the outermost valence region, with the result that NNM occur now in sodium and potassium for the range 5.5–7 bohr (Na) and 8.5–9 bohr (K), approximately. The effect is clearly seen in Fig. 7, which corresponds to potassium. The curvatures of rubidium and cesium are also lowered by the self-consistent and correlation effects, but ρ''_{yy} and ρ''_{zz} remain always positive for the valence regions of both atoms.

Henceforth, the analysis of the promolecular and cluster models explains the behavior of all five alkaline metals. The electron density properties of the bcc bulk metals are in close agreement with the behavior of the M_2 and M_4 homoatomic groups. Lithium and sodium present NNM in the bulk like their respective diatomic molecules and M_4 clusters, even though a small pressure must be applied to bcc sodium before the trend to form NNM can be made evident. Potassium shows shallow NNM because the M_4 group around Wyckoff's 12*d* position tends heavily to accumulate electron density in its baricenter, but the phenomenon is marginal, and the charge accumulated in the NNM is negligible. Finally, the trend implicit in their diatomic molecules dominates the behavior of bulk rubidium and cesium, that lack NNM.

On the other hand, the comparison of the topological trends shown in Figs. 2 and 4 indicates that the alkaline metals can be classified in three different groups: lithium is a case by itself, with special properties like the M_g and M_L topologies; sodium and potassium form the second group, the differences between both crystals being basically a question of degree; finally, rubidium and cesium form the third group. It is suggestive that these groups correspond to differences in the orbital occupation: *s* orbitals are the only ones complete or partially filled in lithium; *s* and *p* core levels are filled in sodium and potassium; and rubidium and cesium are the only ones containing *d* semicore levels. Therefore, whereas all alkali metals behave similarly because all present the same half-filled valence *s* orbital, the differences in their semicore and core levels give rise to non-negligible topological differences among them. This classification, on the other hand, should hardly be a surprise, as it is typical in most systematic classifications of the physical and chemical properties of molecules containing alkaline elements.[52]

Our crystal calculations and our discussion has been limited to the bcc structure of the alkaline metals, which is the phase experimentally found under room conditions. However, all alkaline metals suffer phase transitions when the temperature changes or the pressure is increased. We should expect that these structural modifications would influence the actual occurrence of NNM. However, the qualitative agreement between the crystal and molecular behavior leads us to be confident that our main conclusions regarding the bcc phase will be translated essentially to the other metastable structures. We have seen that the internuclear separation controls the topological change and, accordingly, we should compare geometries with equivalent nearest neighbors separations.

A final word of caution is due regarding the comparison of our results with the experimental topologies. None of our calculations includes the effect of thermal agitation nor zero point effects. Rather, all the electron densities analyzed here, like all the theoretical densities analyzed in the literature so far, correspond to a static model that would differ from the experimental densities, even at the 0 K limit. We expect the thermal effects to be small, but this is a question that requires further research.

V. CONCLUSIONS

We can conclude that metallic lithium presents NNM for a large range of internuclear distances that includes the equilibrium geometry under room conditions. Sodium has also a clear tendency towards NNM, but it appears that a small compression, of the order of 1–2 GPa under room temperature, is needed before they might be found in the bcc phase. Our results thus agree with and extend the recent calculations by Madsen *et al.*[22] Potassium, on the other hand, has a marginal tendency to show NNM and, in fact, the charge accumulated by the possible NNM would be negligible in any case. Rubidium and cesium, finally, should lack NNM for any reasonable geometry. In any case, all alkaline metals share a common tendency towards easy topological change that makes these systems stand completely apart from the prototypical behavior of covalent, ionic, and molecular crystals. In addition, we have ratified the usefulness of the electron density flatness,[28] f, to characterize the metallic state as well as monitoring and comparing diferent computational techniques.

ACKNOWLEDGMENTS

We thank the Spanish Ministerio de Ciencia y Tecnología for financial support under Project No. BQU2000-0466. P.M.S. is currently a Fulbright fellow. A.C.C. is a Ramón y Cajal fellow.

[1] S. Besnainou, M. Roux, and R. Daudel, Compt. Rend. **241**, 311 (1955).
[2] R. F. W. Bader, T. T. Nguyen-Dang, and Y. Tal, Rep. Prog. Phys. **44**, 893 (1981).
[3] R. F. W. Bader, T. S. Slee, D. Cremer, and E. Kraka, J. Am. Chem. Soc. **105**, 5061 (1983).
[4] M. A. Spackman and E. N. Maslen, J. Phys. Chem. **90**, 2020 (1986).
[5] C. Gatti, P. Fantucci, and G. Pacchioni, Theor. Chim. Acta **72**, 433 (1987).
[6] W. L. Cao, C. Gatti, P. J. Macdougall, and R. F. W. Bader, Chem. Phys. Lett. **141**, 380 (1987).
[7] J. Cioslowski, J. Phys. Chem. **94**, 5496 (1990).
[8] R. Glaser, R. F. Waldron, and K. B. Wiberg, J. Phys. Chem. **94**, 7357 (1990).
[9] K. E. Edgecombe, R. O. Esquivel, V. H. Smith, and F. Mullerplathe, J. Chem. Phys. **97**, 2593 (1992).
[10] G. I. Bersuker, C. Y. Peng, and J. E. Boggs, J. Phys. Chem. **97**, 9323 (1993).
[11] C. J. Mei, K. E. Edgecombe, V. H. Smith, and A. Heilingbrunner, Int. J. Quantum Chem. **48**, 287 (1993).
[12] M. Sakata and M. Sato, Acta Crystallogr., Sect. A: Found. Crystallogr. **A46**, 263 (1990).

[13] T. Saka and N. Kato, Acta Crystallogr., Sect. A: Found. Crystallogr. **A42**, 469 (1986).
[14] B. B. Iversen, F. K. Larsen, M. Souhassou, and M. Takata, Acta Crystallogr., Sect. B: Struct. Sci. **B51**, 580 (1995).
[15] F. K. Larsen and N. K. Hansen, Acta Crystallogr., Sect. B: Struct. Sci. **B40**, 169 (1984).
[16] R. Y. de Vries, W. J. Briels, and D. Feil, Phys. Rev. Lett. **77**, 1719 (1996).
[17] B. B. Iversen, J. L. Jensen, and J. Danielsen, Acta Crystallogr., Sect. A: Found. Crystallogr. **A53**, 376 (1997).
[18] D. Jayatilaka, Phys. Rev. Lett. **80**, 798 (1998).
[19] A. M. Pendás, M. A. Blanco, A. Costales, P. Mori-Sánchez, and V. Luaña, Phys. Rev. Lett. **83**, 1930 (1999).
[20] R. Dovesi, V. R. Saunders, C. Roetti, M. Causà, N. M. Harrison, R. Orlando, and E. Aprà, *Crystal95 User's Manual* (1996).
[21] P. Mori-Sánchez, Tesis doctoral, Universidad de Oviedo, Oviedo, Spain 2002 ⟨http://www.uniovi.es/~quimica.fisica/qcg/pms/tesis.html⟩.
[22] G. K. H. Madsen, P. Blaha, and K. Schwarz, J. Chem. Phys. **117**, 8030 (2002).
[23] R. F. W. Bader and J. A. Platts, J. Chem. Phys. **107**, 8545 (1997).
[24] G. K. H. Madsen, C. Gatti, B. B. Iversen, L. Damjanovic, G. D. Stucky, and V. I. Srdanov, Phys. Rev. B **59**, 12359 (1999).
[25] P. Mori-Sánchez, J. M. Recio, B. Silvi, C. Sousa, A. M. Pendás, V. Luaña, and F. Illas, Phys. Rev. B **66**, 075103 (2002).
[26] D. J. Singh, H. Krakauer, C. Haas, and W. E. Pickett, Nature (London) **365**, 39 (1993).
[27] M. F. Crommie, C. P. Lutz, and D. M. Eigler, Science **262**, 218 (1953).
[28] P. Mori-Sánchez, A. M. Pendás, and V. Luaña, J. Am. Chem. Soc. **124**, 14721 (2002).
[29] T. Koga, H. Tatewaki, and A. J. Thakkar, Phys. Rev. A **47**, 4510 (1993).
[30] T. Koga and A. J. Thakkar, Phys. Rev. A **48**, 4775 (1993).
[31] T. Koga and A. J. Thakkar, Phys. Rev. A **50**, 891 (1994).
[32] R. Dovesi, V. R. Saunders, C. Roetti, M. Causà, N. M. Harrison, R. Orlando, and C. M. Zicovich-Wilson, *CRYSTAL98 User's Manual* (1998) ⟨http://www.chimifm.unito.it/teorica/crystal/crystal.html⟩.
[33] P. Blaha, K. Schwarz, and J. Luitz, *WIEN97, a Full Potential Linearized Augmented Plane Wave Package for Calculating Crystal Properties*, edited by K. Schwartz (Technical University Wien, Vienna, 1999), ISBN 3-9501031-0-4; updated version of P. Blaha, K. Schwarz, P. Sorantin, and S. B. Trickey, Comput. Phys. Commun. **59**, 399 (1990).
[34] J. P. Perdew and Y. Wang, Phys. Rev. B **45**, 13244 (1992).
[35] J. P. Perdew, S. Burke, and M. Ernzerhof, Phys. Rev. Lett. **77**, 3865 (1996).
[36] J. P. Desclaux, Comput. Phys. Commun. **1**, 216 (1969).
[37] D. D. Koelling and B. N. Harmon, J. Phys. C **10**, 3107 (1977).
[38] A. Martín Pendás and V. Luaña, *The Critic Program* (1995–2003).
[39] R. F. W. Bader, *Atoms in Molecules. A Quantum Theory* (Oxford University Press, Oxford, 1990).
[40] A. M. Pendás, A. Costales, and V. Luaña, Phys. Rev. B **55**, 4275 (1997).
[41] V. Luaña, A. Costales, and A. M. Pendás, Phys. Rev. B **55**, 4285 (1997).
[42] V. Luaña, A. Costales, P. Mori-Sánchez, and A. Martín Pendás, J. Phys. Chem. B **107**, 4912 (2003).
[43] R. W. G. Wyckoff, *Crystal Structures* (Wiley Interscience, New York, 1963), Vol. I.
[44] R. Berliner and S. A. Werner, Phys. Rev. B **34**, 3586 (1986).
[45] M. S. Anderson and C. A. Swenson, Phys. Rev. B **31**, 668 (1985).
[46] R. Thom, *Structural Stability and Morphogenesis* (Benjamin, Reading, MA, 1975); translated from *Stabilité Structurelle et Morphogénèse* (1972).
[47] E. Francisco, M. A. Blanco, and G. Sanjurjo, Phys. Rev. B **63**, 094107 (2001).
[48] M. Spackman and E. N. Maslen, Acta Crystallogr., Sect. A: Found. Crystallogr. **A40**, C172 (1984).
[49] R. O. Esquivel, J. Chen, M. J. Stott, R. P. Sagar, and V. H. Smith, Jr., Phys. Rev. A **47**, 936 (1993).
[50] R. O. Esquivel, R. P. Sagar, V. H. Smith, Jr., J. Chen, and M. J. Stott, Phys. Rev. A **47**, 4735 (1993).
[51] A. Costales, M. A. Blanco, P. Mori-Sánchez, V. Luaña, and A. Martín Pendás, J. Am. Chem. Soc. (to be published).
[52] N. N. Greenwood and A. Earnshaw, *Chemistry of the Elements*, 2nd ed. (Buterworth Heinemann, Oxford, 1998).
[53] V. Luaña, *Tessel version 2* (1997–2003) ⟨available from: http://www.uniovi.es/~quimica.fisica/qcg/src/tessel.html⟩.
[54] S. Anger *et al.*, *POV-Ray: Persistence of the Vision Ray Tracer* (1997) ⟨available from http://www.povray.org⟩.
[55] M. Phillips, T. Munzner, and S. Levy, *Geomview* (1995) ⟨available from http://www.geomview.org⟩.
[56] T. H. Dunning, J. Chem. Phys. **55**, 716 (1971).
[57] M. J. Frisch, J. A. Pople, and J. S. Binkley, J. Chem. Phys. **80**, 3265 (1984).
[58] A. D. McLean and G. S. Chendler, J. Chem. Phys. **72**, 5639 (1980).
[59] A. J. H. Wachters, J. Chem. Phys. **52**, 1033 (1970).
[60] K. D. Dobbs and W. J. Hehre, J. Comput. Chem. **8**, 880 (1987).
[61] E. D. Glendening, D. Feller, and M. Thompson, J. Am. Chem. Soc. **116**, 10657 (1994).
[62] E. D. Glendening and D. Feller, J. Phys. Chem. **99**, 3060 (1995).
[63] M. J. Frisch, G.W. Trucks, H. B. Schlegel *et al.*, GAUSSIAN 98, Revision A.6, Gaussian, Inc., Pittsburgh, PA, 1998.
[64] R. W. F. Bader's Laboratory, *AIMPAC* (1989) ⟨available from: http://www.chemistry.mcmaster.ca/aimpac/⟩.
[65] M. W. Schmidt, K. K. Baldridge, J. A. Boatz *et al.*, J. Comput. Chem. **14**, 1347 (1993).